Environmental Science
Water Research & Technology

ROYAL SOCIETY OF CHEMISTRY

PAPER

View Article Online
View Journal | View Issue

Cite this: *Environ. Sci.: Water Res. Technol.*, 2024, **10**, 639

Antimicrobial activity of thin-film composite membranes functionalized with cellulose nanocrystals and silver nanoparticles *via* one-pot deposition and layer-by-layer assembly†

Jennifer C. Jackson,[a] Camilla H. M. Camargos,[bc] Caihong Liu,[d] Diego S. T. Martinez,[e] Amauri J. Paula,[fg] Camila A. Rezende[b] and Andreia F. Faria*[a]

Received 9th November 2023,
Accepted 9th January 2024

DOI: 10.1039/d3ew00826f

rsc.li/es-water

In this study, we propose the production of a thin-film composite (TFC) membrane with efficient antimicrobial properties by modifying it with cellulose nanocrystals (CNC) and silver nanoparticles (AgNP). Two approaches (*i.e.*, "one-pot" and "layer-by-layer") were employed to incorporate CNC and AgNP onto the membrane surface and their impact on the membrane antimicrobial properties was examined. Firstly, the "one-pot" method involved reacting CNC with $AgNO_3$ and $NaBH_4$ to form a CNC/Ag hybrid material. This CNC/Ag hybrid was then applied to the TFC drawmembranes using polydopamine (PDA) chemistry, allowing the deposition of both CNC and AgNP in a single step. Secondly, the "layer-by-layer" method involved attaching CNC to the membrane surface using PDA chemistry, which was then followed by an *in situ* reaction of $AgNO_3$ and $NaBH_4$ to deposit the AgNP directly on top of the CNC layer. Membranes modified with a CNC/Ag hybrid using the one-pot method were able to deactivate 75.7 ± 15.6% of attached *E. coli* cells without detrimental impact to membrane separation performance. The membranes modified using the layer-by-layer assembly demonstrated improved antimicrobial activity when compared to those modified with the one-pot CNC/Ag hybrid, being capable of inactivating 90% of the attached *E. coli* cells. On the other hand, the layer-by-layer modification method led to a significant loss in the membrane's salt rejection capacity. These water-based, straightforward, and simple functionalization strategies can tailor the antimicrobial and anti-biofouling performance of membranes for water treatment applications.

Water impact

The demand for high-quality potable water has increased significantly due to population growth, making seawater desalination a crucial process in many parts of the world. While thin-film composite (TFC) membranes are undoubtedly effective in desalinating water, they face long-term performance limitations such as biofouling and organic fouling. To combat these challenges, this study proposes a sustainable solution that involves the use of cellulose nanocrystals (CNC) to enhance the TFC membrane's ability to resist bacterial attachment, thus increasing the longevity of the membrane and reducing operations costs. Our study uses two techniques, single-pot and layer-by-layer approaches, to functionalize the TFC membrane with CNC and AgNP materials and evaluate which strategy can maximize antimicrobial activity while minimizing changes in water permeability and salt selectivity.

[a] *Engineering School of Sustainable Infrastructure & Environment (ESSIE), Department of Environmental Engineering Sciences, University of Florida, Gainesville, FL, 32611-6580, USA. E-mail: andreia.faria@essie.ufl.edu; Tel: +1 352 392 7104*
[b] *Instituto de Química, Departamento de Físico-Química, Universidade Estadual de Campinas (UNICAMP), P.O. Box 6154, 13083-970, Campinas, São Paulo, Brazil*
[c] *School of Fine Arts, Universidade Federal de Minas Gerais – UFMG, Belo Horizonte, Minas Gerais, 31270-901, Brazil*
[d] *Key Laboratory of Eco-environments in Three Gorges Reservoir Region, Ministry of Education, College of Environment and Ecology, Chongqing University, Chongqing 400044, China*
[e] *Brazilian Laboratory of Nanotechnology, National Center for Research in Energy and Materials – CNPEM, Campinas, São Paulo, 13083-100, Brazil*
[f] *Ilum School of Science, National Center for Research in Energy and Materials – CNPEM, Campinas, São Paulo, 13083-100, Brazil*
[g] *Physics Department, Universidade Federal do Ceará, Fortaleza, Ceará, 60455-900, Brazil*

† Electronic supplementary information (ESI) available: Additional methods, TEM image and size distribution histograms for CNC, a scheme for the bench-scale reverse osmosis filtration system, photos of the pristine and modified membranes, cross-sectional TEM and EDS analysis of functionalized membranes, FTIR and XPS of membranes functionalized with CNC and AgNP, overview of key parameters affected by various approaches applied to membrane functionalization with AgNP, and confocal images and cell counts for the static biofouling assay are provided in the supporting information. See DOI: **https://doi.org/10.1039/d3ew00826f**

Introduction

The availability of potable water on a global scale is facing significant challenges as a result of increasing population, rapid urbanization, environmental pollution, and the impact of climate changes.[1–5] Increasing periods of drought and flooding, saltwater intrusion, urban and agricultural runoff, and aging infrastructure contribute to a decline in drinking water supply quality.[6–9] To address this pressing issue, it will be critical to implement membrane-based water treatment processes to meet the growing demand for high-quality drinking water.[10] Membrane processes have proven effective in removing a wide range of contaminants, including emerging pollutants such as microplastic,[11] pharmaceuticals,[12,13] and per/polyfluoroalkyl substances (PFAS).[14–16] High pressure membrane filtration processes, such as nanofiltration (NF) and reverse osmosis (RO), which utilize thin-film composite (TFC) membranes, are currently the industry standard and have demonstrated the ability to produce high-quality potable water. However, these TFC membranes are known to be susceptible to fouling and require diligent maintenance to ensure optimal performance.

Membrane fouling in feed water is caused by four distinct types of species. The first is particulate fouling, where particulates or colloids accumulate on the membrane surface.[17,18] The second is scaling resulting from precipitation of inorganic salts.[19,20] The third type is organic fouling, which occurs when organic biomacromolecules adsorb on the membrane surface.[21,22] Lastly, biofouling, the most detrimental type, develops when microorganisms proliferate on the membrane surface and release extracellular polymeric substances (EPS).[23,24] Biofouling leads to increased costs, complicates operation, and is often irreversible. Well-formed biofilms reduce membrane performance[25] and protect the microorganisms inside from the chemicals used for cleaning, ultimately resulting in a shorter membrane lifespan and higher operational costs.[26] Furthermore, biofouling is inevitable as membrane filtration is not performed in sterile systems. Over time, microorganisms will accumulate, and biofouling will ensue.

For this reason, antimicrobial membrane modifications have been explored recently to increase membrane lifespan. Membrane modification strategies are typically divided into two categories: "defending" and "attacking" strategies.[27] "Defending" strategies aim to improve the membrane resistance to the adsorption of organic compounds. For instance, membrane surface modification with zwitterionic polymer brushes increases hydrophilicity, which reduces organic compound adsorption and bacterial adhesion.[28,29] "Attacking" strategies involve modifying the membrane surface with substances that are toxic to bacteria, such as functionalized metal–organic framework and clay nanoparticles,[30,31] single-walled carbon nanotubes,[32,33] graphene oxide,[34–36] and nanocellulose.[37] In a previous study, the antimicrobial activity and mechanism of microbial deactivation by cellulose nanocrystals (CNC)[38] was explored for potential application as an "attacking" strategy for improving membrane antimicrobial properties.[39] It was found that CNC require contact with the microorganism as part of a physical-stress related mechanism of microbial deactivation.[38]

However, CNC as a coating only target the initial layer of bacteria that will be directly exposed to the nanomaterial on the surface.[40] Once an initial layer of bacteria has formed on the membrane surface, they can provide a conditioning layer that will prevent further bacteria from contacting CNC on the membrane surface.[41] To overcome this limitation, hybridization of CNC with another nanomaterial, such as silver nanoparticles (AgNP), has been explored.[40,42,43] AgNP have been chosen for this proof of concept as their microbial toxicity and mechanisms of microbial deactivation are well-established.[44–48] Hybridization of CNC with toxic metallic AgNP has proven to be an effective way to enhance the antimicrobial properties of CNC, increasing their ability to inactivate bacteria in both aqueous environments and on surfaces.[49,50] This approach is especially advantageous for inactivating planktonic bacteria cells in aqueous media, where CNC displays limited toxicity.[38,51] AgNP have the ability to release biocidal Ag^+ ions into the bulk solution, overcoming the need for direct contact between the microorganisms and the CNC. In addition, CNC provide a large surface area for nucleation of silver, which favors the anchoring of silver nanoparticles while preventing agglomeration.[52,53] The hydroxyl functional groups present on the CNC surface facilitate AgNP nucleation through ion-dipole interactions.[54] Native hydroxyl and carboxyl functional groups on the CNC surface also provide anchoring sites for the deposition of Ag clusters and nanoparticles.[52] The association between AgNP and CNC enhances the toxicity of CNC, expanding its use as an anti-biofouling agent. Another advantage of using CNC/Ag hybrids is the residual toxicity of CNC. After depleting the AgNP, the remaining non-leachable and antimicrobial CNC can still impart toxicity to the surface.

To perform these necessary modifications on TFC membranes, we present here new, water-based, and relatively cost-effective approaches for modifying TFC membranes with CNC and AgNP utilizing polydopamine (PDA) chemistry. While one objective of this work is to modify the membrane surface to achieve antimicrobial properties, it is essential that membrane performance is not compromised by this process. For this reason, two different approaches of applying the CNC and AgNP to membrane surface were explored in this work: the "one-pot" and "layer-by-layer" methods. In the "one-pot" method, AgNP are nucleated on CNC in suspension to form a CNC/Ag hybrid that is then applied to the membrane surface using PDA chemistry. The "one-pot" procedure has the methodological advantage of protecting the TFC membrane surface from exposure to sodium borohydride (a strong reducing agent) during the reaction to reduce Ag^+ ions into Ag^0. In the "layer-by-layer" method, CNC are first applied to the membrane surface using PDA

chemistry and then AgNP are nucleated on top of the CNC layer through reduction of Ag^+ by sodium borohydride. The modified membranes were characterized regarding their morphological, antimicrobial, and filtration properties so as to draw comparisons between these two methods.

Materials and methods

Chemicals and materials

Silver nitrate (certified ACS, ≥99.0%), sodium borohydride (99%), sodium bromide (≥99%), and (2,2,6,6-tetramethylpiperidin-1-yl)oxyl (TEMPO, 98%) were obtained from Sigma-Aldrich (St. Louis, MO, USA). Sodium chloride (crystalline/certified ACS, ≥99.0%), lysogeny broth (LB), agar (powder/flakes), sodium phosphate dibasic (anhydrous, certified ACS, 98.0 to 100.5% (USP)), sodium phosphate monobasic (anhydrous, 99%), ethanol (absolute, 200 proof, Molecular Biology Grade, ≥99.5%), 3-hydroxytyramine hydrochloride (99%), tris(hydroxymethyl) aminomethane (Tris base, ≥99.8%) were obtained from Fisher Scientific (Atlanta, GA, USA). A LIVE/DEAD™ BacLight™ bacterial viability kit was obtained from Thermo Fisher Scientific (Carlsbad, CA, USA). Glutaraldehyde (50% aqueous solution, Electron Microscopy Grade), paraformaldehyde (16% aqueous solution, Electron Microscopy Grade), and hexamethyldisilazane (97.0%) were obtained from Electron Microscopy Sciences (Hatfield, PA, USA). Sulfuric acid (H_2SO_4, 98%) and sodium hydroxide (NaOH, certified ACS, 99.0%) were obtained from Synth (Diadema, SP, Brazil). Sodium chlorite (NaClO, 10–12%) was obtained from Êxodo Científica (Sumaré, SP, Brazil). Elephant grass (*Pennisetum purpureum*) was kindly supplied by the Institute of Animal Science (Instituto de Zootecnia, Nova Odessa, São Paulo, Brazil). Plants were harvested twelve months after planting. Leaves were separated, dried in a convection oven (Tecnal TE-394/3, Piracicaba, SP, Brazil) at 60 °C for 24 h, and knife milled through a 10-mesh sieve (grinder SOLAB – SL 31, Piracicaba, SP, Brazil). After, the milled biomass was stored in plastic bags. Thin-film composite membranes (FilmTec Flat Sheet SW30XLE membrane) were obtained from OctoChem (Vandalia, IL, USA). Deionized (DI) water with a resistance of 18.2 MΩ cm was obtained from a Milli-Q® Direct water purification system (EMD Millipore, Burlington, MA, USA). All solutions described were prepared using deionized water.

Preparation of cellulose nanocrystals

Cellulose nanocrystals (CNC) were prepared from the leaves of elephant grass (*Pennisetum purpureum*), which were previously subjected to a two-step hydrothermal treatment using diluted sulfuric acid (1%, v/v) and sodium hydroxide (2%, w/v) aqueous solutions (Fig. 1). Both the acid and alkali steps were conducted at 121 °C and 1.05 bar, following a method previously reported.[55] The pretreated biomass was then oxidized with sodium hypochlorite in the presence of TEMPO and sodium bromide. TEMPO-mediated oxidation was followed by probe-sonication to directly prepare CNC with an oxygen-rich surface, and a needle-like morphology, with average length of 159 ± 81 nm and diameter of 5 ± 2 nm (Fig. S1†). A more detailed description of the procedure to produce the TEMPO-oxidized CNC can be found in our previous studies.[38,39] The aqueous dispersions of CNC were stored in aqueous suspensions at 4 °C until use.

Preparation of CNC/Ag

The production of CNC/Ag involved the utilization of CNC derived from elephant grass leaves (Fig. 1), following methodologies previously described for microcrystalline cellulose-derived CNC.[56,57] Briefly, 25 mL of a 1000 μg mL^{-1} CNC dispersion was prepared by resuspending an aliquot of the stock dispersion into DI water through bath sonication. Silver nitrate was added to the CNC dispersion to obtain an $AgNO_3$ concentration of 10 mM. The mixture was stirred for an hour and then centrifuged for 10 minutes at 17 000 rpm using an Allegra 64R centrifuge (Beckman Coulter, Brea, CA), after which the supernatant was discarded and the CNC pellet was resuspended in 22.5 mL of fresh DI water. While stirring, 2.5 mL of aqueous 10 mM $NaBH_4$ solution was then added to the CNC dispersion drop-wise to synthesize the AgNP. As $NaBH_4$ was added to the solution, the color changed to dark brown indicating the presence of AgNP. The dispersion of CNC/Ag was then stirred overnight in darkness and then collected in a 3.5 kDa molecular weight cut-off (MWCO) dialysis membrane (Spectra/Por membrane, Spectrum Laboratories, USA). After dialysis for 2 hours in DI water, the CNC/Ag suspension was stored at 4 °C until use.

Characterization of the CNC/Ag

We used transmission electron microscopy (TEM) to evaluate the morphological characteristics of CNC/Ag. A 400-mesh carbon-coated Formvar nickel grid was glow discharged using the PELCO easiGlow (Ted Pella, Redding, CA). A 10 μL droplet of the provided CNC/Ag sample was placed on the top of the TEM grid for 5 minutes and the excess solution was drawn off with filter paper. Another 10 μL droplet of 0.5% aqueous uranyl acetate was then placed on the top of the grid for 30 seconds. After removing the excess stain with filter paper, the sample was air dried and examined with an FEI Tecnai G2 Spirit Twin TEM (FEI Corp., Hillsboro, OR). Digital images were acquired with a Gatan UltraScan 2k × 2k camera and Digital Micrograph software (Gatan Inc., Pleasanton, CA). The size of AgNP particles nucleated on the CNC was measured using TEM images analyzed with ImageJ software. The size distribution shown for the AgNP is based on the measurements for 223 particles.

The chemical properties of the CNC and CNC/Ag were evaluated using X-ray photoelectron spectroscopy (XPS). For this, suspensions of CNC and CNC/Ag were lyophilized to yield a solid, and the analysis was conducted with a PHI VersaProbe III Scanning XPS Microprobe (Physical Electronics, Chanhassen, MN, USA) using a monochromatic Al-Kα X-ray source ($h\nu$ = 1486.7 eV). The photoelectron escape

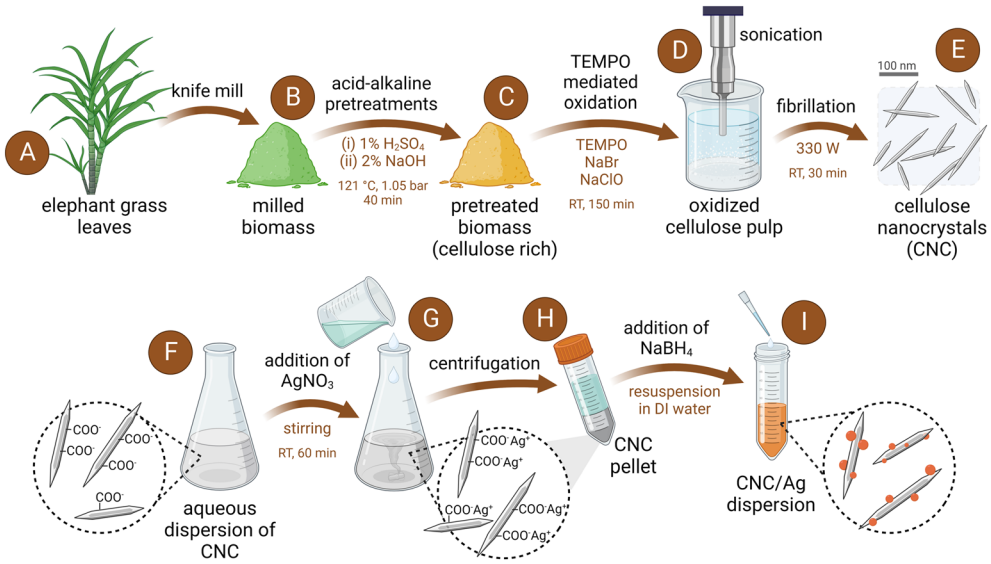

Fig. 1 Illustration of the preparation of CNC from elephant grass leaves and the subsequent preparation of the CNC/Ag hybrid. (A) Elephant grass leaves are knife-milled and (B) pretreated using alkaline and acidic conditions. (C) The pretreated biomass is subjected to TEMPO-mediated oxidation and (D) sonicated to yield the (E) CNC. (F) An aqueous dispersion of CNC is stirred with $AgNO_3$ for 60 minutes, (G) after which the suspension is centrifuged and the supernatant discarded. (H) The pellet is resuspended in DI water and exposed to $NaBH_4$ to produce the (I) CNC/Ag hybrid.

depth was less than 10 nm and the takeoff angle for the photoelectrons was set to 45°. XPS analysis was conducted over an area of 100 μm^2 and the spectra were averaged over 5 scans.

"One-pot" and "layer-by-layer" membrane functionalization

The membrane surface was treated with nanomaterials using a polydopamine (PDA) reaction method from previous studies.[58,59] Firstly, the commercial TFC membranes (FilmTec Flat Sheet SW30XLE) were clamped in a holder to expose only the polyamide active layer and then placed on an orbital shaker at 30 rpm for the entire functionalization process. Next, a solution of 2 g L^{-1} dopamine hydrochloride (DH) dissolved in 10 mM Tris base at pH 8.5 was applied to the membrane for 15 min. The thickness of the PDA layer formed on a surface depends on the time the surface is exposed to the buffered DH solution.[58] 15 minutes was used to create a thin layer of PDA on the TFC membrane surface. Afterward, the solution was discarded, and the membrane was rinsed briefly with DI water. Membranes modified with only a thin layer of PDA are referred to as TFC-PDA. To apply CNC to the membrane, a coupon of TFC-PDA was contacted with a suspension of 500 μg mL^{-1} CNC in 10 mM Tris base at pH 8.5 for 24 h. This step allowed the CNC to attach to the PDA layer. Membranes modified with a thin layer of PDA and CNC are referred to as TFC-CNC. An illustration of this method is shown in Fig. 2.

After forming the initial PDA layer, the TFC-PDA membrane coupons were contacted with a suspension of CNC/Ag in 10 mM Tris base at pH 8.5 for 24 h to attach the CNC/Ag to the PDA layer. This method of applying CNC/Ag to the TFC membrane is referred to as the "one-pot" method as both CNC and AgNP were added in one step. Membranes modified with CNC/Ag hybrid in this way using PDA chemistry were referred to as TFC-OP (Fig. 2).

Following the binding of CNC to the membrane surface for 24 h, AgNP were deposited on the surface of TFC-CNC membranes using an *in situ* reaction. The TFC-CNC was contacted with 15 mL of 5 mM $AgNO_3$ for 1 h. The $AgNO_3$ solution was then removed, and the membrane was not rinsed before being treated with 15 mL of 5 mM $NaBH_4$ to convert the Ag^+ adsorbed onto the membrane surface into metallic AgNP. The $NaBH_4$ solution was allowed to remain in

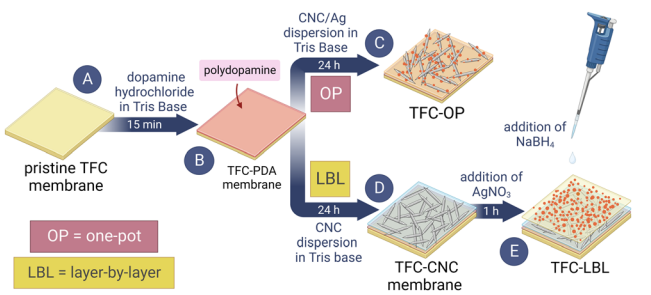

Fig. 2 Illustration showing the "one-pot" (OP) (upper path) and "layer-by-layer" (LBL) (lower path) methods for applying CNC and AgNP to the TFC membrane surface using PDA chemistry to attach the nanomaterials. (A) Commercial TFC membranes are exposed to dopamine hydrochloride in Tris base to form (B) a PDA layer on the membrane surface. In the "one-pot" method, following initial PDA deposition, (C) the membrane is contacted with CNC/Ag dispersed in Tris base to attach CNC/Ag to the PDA layer (TFC-OP). In the "layer-by-layer" method, following initial PDA deposition, (D) the membrane is contacted with CNC dispersed in Tris base to attach CNC to the PDA layer (TFC-CNC). (E) AgNP is then formed on the TFC-CNC membrane using a reaction *in situ* with $AgNO_3$ and $NaBH_4$ (TFC-LBL).

contact with the membrane surface for 10 min before being discarded. This two-step process is referred to as the "layer-by-layer" method, as each nanomaterial (CNC and AgNP) was applied separately. Membranes modified in this manner are abbreviated as TFC-LBL (Fig. 2).

Membrane characterization

Scanning electron microscopy (SEM) was employed to observe the morphological features of both pristine and modified membrane surfaces. To prepare the samples for SEM, membrane coupons of 1 cm^2 were dried overnight in a vacuum desiccator at room temperature and then attached to aluminum SEM stubs using conductive carbon tape. The SEM stubs were subsequently dried overnight in a vacuum desiccator and sputter-coated with a mixture of gold and palladium in a Denton V Sputter Coater. SEM micrographs of the membrane surface were obtained in a Hitachi SU5000 Schottky Field-Emission Scanning Electron microscope at an accelerating voltage of 5 kV. Morphological characteristics and elemental composition of the two functionalized membranes (TFC-OP and TFC-LBL) were characterized using energy dispersive spectrometry (EDS) during TEM cross-sectional imaging. TEM measurements were conducted using a Talos F200S with an accelerating voltage of 200 kV. Before imaging, the membrane samples were embedded inside blocks of epoxy resin and cut by a diamond knife using ultramicrotomy (Leica EM UC7) to obtain membrane cross-sections.

To determine the surface hydrophilicity of pristine TFC and CNC-functionalized membranes, the sessile drop method with DI water was utilized. Membrane coupons were attached to glass microscope slides and dried overnight at room temperature before contact angle measurements were taken using a Ramé-Hart contact angle goniometer and DROPImage software. The results are presented as an average of 60 measurements taken at random locations on 2 different membrane coupons. The intrinsic water transport properties of the pristine and modified membranes, such as water permeability (A) and solute permeability (B), were evaluated in a laboratory-scale crossflow reverse osmosis system (Fig. S2†) following the procedures carefully described in our previous study.[39] The system was operated at 400 psi with a crossflow velocity of 20 cm s^{-1} and samples were tested in triplicate.

Atomic force microscopy (AFM) was performed to observe the surface topography and roughness of the pristine and modified TFC membranes. Samples were cut into 10 × 10 mm squares and fixed with double-sided tape over a metal plate. 10 × 10 μm areas were scanned using an NX-10 (ParkSystems) microscope operating in tapping mode at a scan rate of 0.3 Hz, using a probe with a spring constant of 2.8 N m^{-1}, and resonance frequency of 75 kHz. Images were processed and analyzed using Gwyddion® software (v. 2.53) to obtain average area roughness parameters such as root-mean-square height (S_q) and arithmetical mean height (S_a).

The presence of CNC and AgNP on the surface of the TFC membrane was evaluated using a Fourier transform infrared spectrometer operating in attenuated total reflection mode (FTIR-ATR). Spectra of samples were acquired from 400–4000 cm^{-1} with a resolution of 4 cm^{-1} averaged over 100 scans using an IRSpirit ATR-FTIR (QATR-S, Shimadzu, Brazil). Membrane coupons were dried in a vacuum desiccator prior to FTIR analysis. The chemical binding of CNC and AgNP to the membrane surface was evaluated using XPS following the methods previously described for the samples of dried CNC and CNC/Ag. Membranes were dried overnight in a vacuum desiccator and the analysis was conducted with a PHI VersaProbe III Scanning XPS Microprobe (Physical Electronics, Chanhassen, MN, USA).

Silver leaching from functionalized membranes

In order to assess the amount of silver that can be released from the modified membranes, a silver leaching experiment was conducted using techniques from a previous study.[60] Small coupons (1 cm^2) of the TFC-OP and TFC-LBL membranes were placed into tubes containing 10 mL of 5 mM $NaHCO_3$ at pH 8.3 and agitated continuously. The membranes were removed at specific time intervals and transferred to new tubes containing 10 mL of 160 mM HNO_3 to dissolve the residual silver on the membrane coupon. The silver content of the suspension was then quantified by inductively coupled plasma mass spectrometry (ICP-MS).

Antimicrobial activity determination

The antimicrobial property of the CNC-functionalized membrane was assessed by a plate counting method. A suspension of *Escherichia coli* cells (American Type Culture Collection Strain 8739) at a concentration of 10^8 colony-forming units per mL (CFU mL^{-1}) was contacted with the membrane surface (3 mL cm^{-2}) for 3 h at room temperature. After this time, the suspension was discarded, and the membrane coupons were washed with sterile saline (0.9% NaCl). The bacteria cells were detached from the membrane surface by bath sonication for 15 minutes and then quantified using a plate counting method. Serial dilutions were prepared from the bacteria suspension, spread on LB agar plates, and incubated overnight at 37 °C. Additionally, the viability of *E. coli* cells attached to the membrane surface following the 3-hour contact time was quantified using fluorescent staining with SYTO 9 (live cells) and propidium iodide (PI, dead cells). The membranes stained with these fluorescent labels were observed using confocal microscopy. A more detailed description of this procedure is provided in the ESI.†

Characterization of morphology of bacteria on membrane surface

To examine the morphological characteristics of the bacteria cells attached to the membrane surface, suspensions of *E. coli* were prepared according to the method described above.

After contacting the membrane surfaces with the bacterial suspension, the membrane coupons were fixed using Karnovsky's fixative and prepared for SEM imaging following the procedures described in our previous studies.[38,39]

Antimicrobial activity of membranes following silver leaching

Large coupons of the TFC-OP and TFC-LBL membranes were stirred for 2 weeks in 5 mM $NaHCO_3$ with the goal to lixiviate silver from the membrane surface. Each day the $NaHCO_3$ solution was discarded and replaced with fresh 5 mM $NaHCO_3$. After the 2 weeks were concluded, the membranes were thoroughly rinsed with DI water and then tested against *E. coli* following the previously described method. The surface of leached membranes and a pristine TFC control were contacted with 10^8 CFU mL^{-1} *E. coli* suspension (3 mL cm^{-2}) for 3 h at room temperature. Afterward, the suspension was discarded, and the membrane coupons were washed with sterile saline. The membrane coupons were then bath-sonicated for 15 minutes to detach the bacteria from the membrane surface. Serial dilutions were prepared from the bacteria suspension, spread on LB agar plates, and incubated overnight at 37 °C.

Results and discussion

Physicochemical characterization of CNC/Ag

The CNC/Ag hybrid material was synthesized using the reduction of $AgNO_3$ by $NaBH_4$. In the TEM micrograph in Fig. 3A, small AgNP nucleated on the CNC are shown as black spots. These TEM micrographs were also used to estimate the size of the AgNP and the average diameter of the AgNP was 7.0 ± 2.8 nm (Fig. 3B). XPS analysis was performed on a lyophilized sample of the CNC/Ag hybrid material and in a sample of lyophilized CNC that was tested for comparison (Fig. 3C–F). In the high-resolution Ag 3d spectra for CNC/Ag (Fig. 3F), the peak located at a binding energy of 368.9 eV was attributed to Ag $3d_{5/2}$ while the peak located at a binding energy of 374.9 eV was attributed to Ag $3d_{3/2}$. The 6.0 eV binding energy separating this couplet is indicative of the presence of metallic silver[61,62] in the CNC/Ag hybrid material.

Characterization of functionalized membranes

Commercial TFC membranes were modified using well-established PDA chemistry. The thin PDA layer initially formed on the TFC surface does not impart a visible color to the membrane surface (Fig. S3B†), nor does the deposition of CNC afterward (Fig. S3C†). AgNP appear brown in CNC/Ag dispersion, and this color is visible and manifested when the hybrid material is attached to the TFC membrane surface (Fig. S3D†), indicating the incorporation of AgNP on the membrane surface. A similar color trend is observed for TFC membranes modified with CNC and AgNP *via* layer-by-layer assembly (Fig. S3E†). The results showing the successful functionalization of the TFC membranes with CNC and AgNP *via* PDA layer deposition can be more clearly observed in the SEM images of the membrane surface (Fig. 4). Agglomerates of PDA and CNC appear as large sheet-like structures

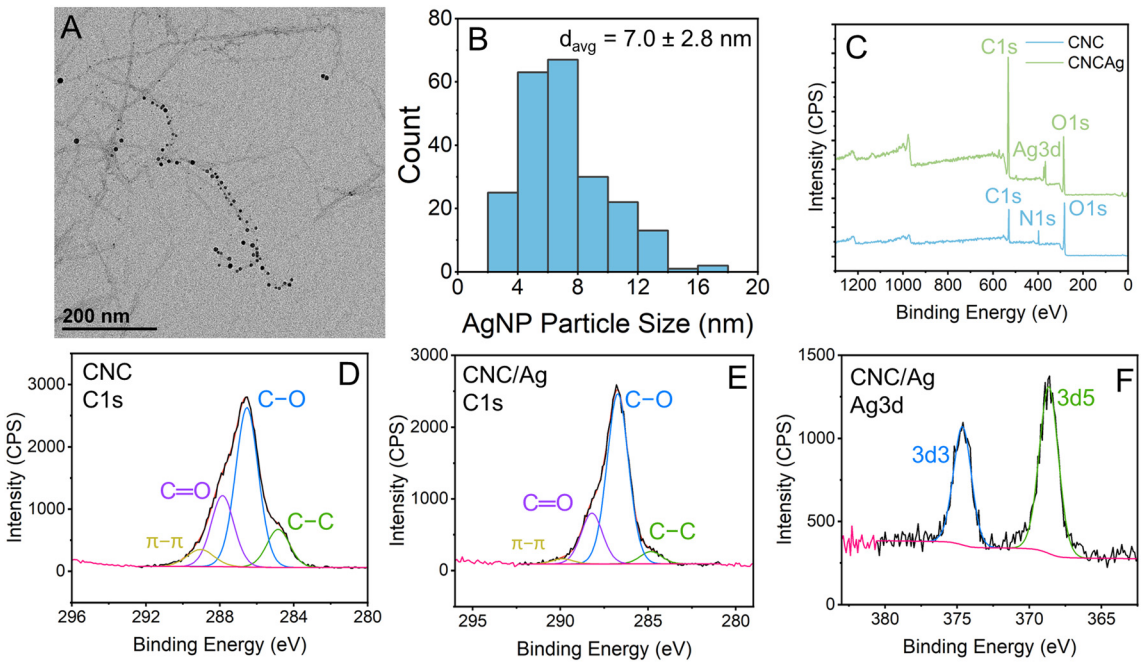

Fig. 3 (A) TEM micrograph of the CNC/Ag hybrid, where AgNP appear as black dots. (B) Size distribution for the AgNP based on measurements taken from 223 AgNP particles in TEM micrographs of the CNC/Ag using ImageJ software, the average diameter of AgNP was 7.0 ± 2.8 nm. (C) XPS full survey spectra for lyophilized CNC and CNC/Ag. High-resolution C 1s spectrum for the CNC (D) and CNC/Ag (E). (F) High-resolution Ag 3d spectrum for the CNC/Ag.

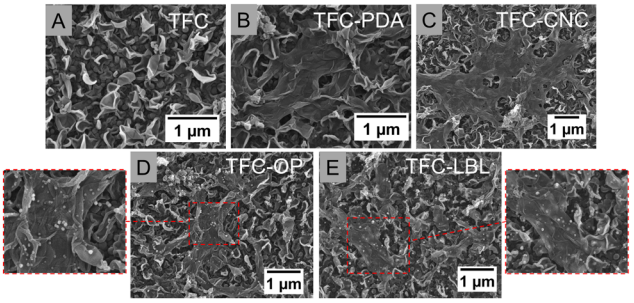

Fig. 4 SEM micrographs of the (A) pristine TFC membrane, (B) membrane modified with only PDA (TFC-PDA), (C) membrane modified with CNC using PDA (TFC-CNC), (D) membrane modified using the "one-pot" method to attach CNC/Ag to the membrane surface with PDA (TFC-OP), and (E) membrane modified using the "layer-by-layer" method to attach CNC to the membrane *via* PDA followed by *in situ* AgNP formation (TFC-LBL). Areas indicated by red rectangles are enlarged to show the AgNP on the membrane surface which appear as white particles in the SEM micrographs.

covering the ridge-and-valley polyamide layer of the TFC membrane surface (Fig. 4B). AgNP are also clearly visible as small bright particles in the micrographs of the TFC-OP (Fig. 4D) and TFC-LBL (Fig. 4E) membranes. EDS analysis used with cross-sectional TEM imaging also confirmed the presence of silver on the membrane surface of TFC-OP and TFC-LBL (Fig. S4†).

Through AFM analysis (as shown in Fig. 5), we observed the topography of both the pristine TFC membranes and those modified with CNC and AgNP using PDA chemistry. Previous studies have shown that TFC membranes had increased tridimensional roughness after being functionalized with CNC *via* amide crosslinking.[39] However, no significant increase in surface roughness was observed when CNC was deposited on the TFC membrane using the PDA self-polymerization reaction (Fig. 5). None of the membranes modified with CNC and/or AgNP using PDA chemistry demonstrated changes in root-mean-square height (S_q) or arithmetical mean height (S_a) that were statistically significantly different from the control pristine TFC membrane at a confidence level of 95% ($\alpha = 0.05$). The root-mean-square height observed for the membranes functionalized with CNC and/or AgNP are close to the lower end of the typical range for TFC membranes (100–200 nm).[63]

The TFC-LBL membrane exhibited a notable increase in surface roughness, with a root-mean-square height of 123.9 ± 11.1 nm and an arithmetical mean height of 96.9 ± 9.2 nm. In contrast, the pristine TFC membrane had a root-mean-square height of 98.3 ± 20.8 nm and an arithmetical mean height of 76.8 ± 13.5 nm. However, the differences in surface roughness between the unmodified and modified membranes were not statistically significant, implying that it could be attributed to the variability in membrane surface roughness across the TFC membrane. It is imperative to note that the AFM analysis was performed on a 10 μm by 10 μm area, providing only a small snapshot of the membrane surface. Modification with CNC and AgNP using the "one-pot" and "layer-by-layer" methods did not significantly increase membrane surface roughness, which has positive implications as surface roughness is a contributing factor to membrane biofouling.[24]

The results of contact angle measurements on pristine and modified membranes are shown in Fig. 6A. These findings suggest that modification with PDA and with CNC improves the hydrophilicity of the TFC membranes. The TFC-PDA and TFC-CNC membranes exhibited water contact angles of 23.9 ± 4.6° and 17.7 ± 3.0°, respectively,

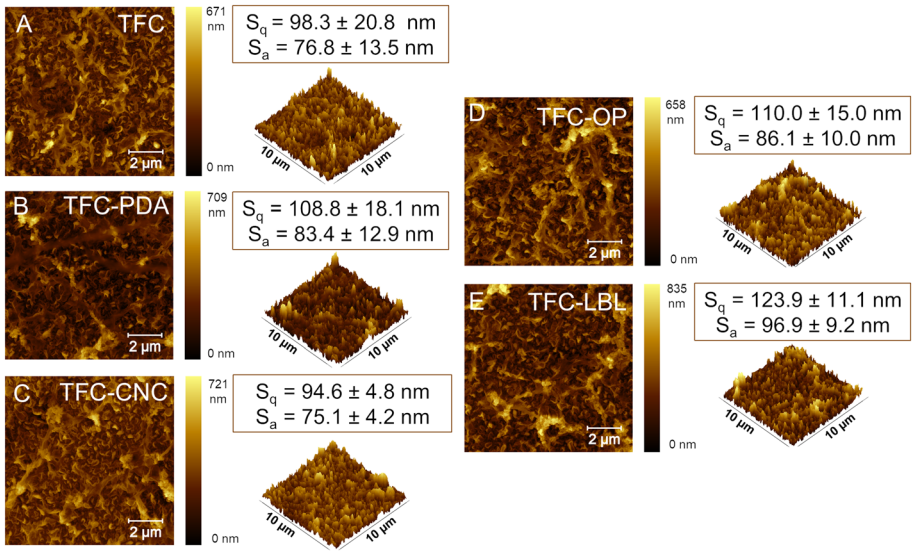

Fig. 5 AFM topography images and 3D roughness mapping for the (A) pristine TFC membrane, (B) membrane modified with only PDA (TFC-PDA), (C) membrane modified with CNC using PDA (TFC-CNC), (D) membrane modified using the "one-pot" method to attach CNC/Ag to the membrane surface with PDA (TFC-OP), and (E) membrane modified using the "layer-by-layer" method to attach CNC to the membrane *via* PDA followed by *in situ* AgNP formation (TFC-LBL).

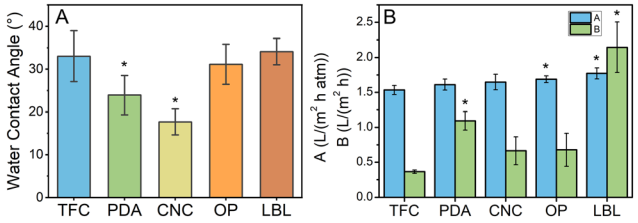

Fig. 6 (A) Water contact angle of the pristine and modified membranes. (B) Intrinsic transport properties of the pristine and modified membranes. *A* refers to the water permeability coefficient and *B* refers to the solute (NaCl) permeability coefficient of the membranes. An asterisk is used to denote samples that were statistically significantly different from the control (pristine TFC) at a confidence level of 95% (α = 0.05).

significantly lower than that of the pristine TFC membrane which had a water contact angle of 33 ± 5.9°. Previous research has demonstrated modification of TFC membranes with CNC using amide coupling also led to an increase in hydrophilicity.[39] The results also suggest that the presence of AgNP on the membrane surface appears to counterbalance the increase in hydrophilicity imparted by PDA and CNC, which could be the result of increased roughness due to the morphology of the AgNP. For example, the TFC-OP and TFC-LBL membranes displayed water contact angles of 34.0 ± 3.0° and 31.1 ± 4.7°, respectively. These values were not significantly different from that of the control, indicating that functionalization with AgNP using these two methods is at least not detrimental to the hydrophilicity of the TFC membrane.

The transport properties of pristine and functionalized TFC membranes were also determined in a bench-scale RO membrane filtration unit and the results are shown in Fig. 6B. The water permeability coefficient, *A*, was statistically significantly increased for both TFC-OP and TFC-LBL compared with the unmodified control. The TFC-OP membrane exhibited a water permeability coefficient of 1.69 ± 0.05 L m^{-2} h^{-1} atm^{-1}, representing a 10.5% increase from the control pristine TFC membrane at 1.52 ± 0.07 L m^{-2} h^{-1} atm^{-1}. The TFC-LBL membrane showed a water permeability coefficient of 1.77 ± 0.08 L m^{-2} h^{-1} atm^{-1}, corresponding to a 15.6% increase from the control pristine TFC membrane. While both methods of applying AgNP to the membrane surface improved water permeability, there were significant differences observed for the salt permeability coefficient, *B*. The salt permeability coefficient of the TFC-OP membrane was 0.68 ± 0.24 L m^{-2} h^{-1} which was not significantly different from that of the pristine TFC membrane (0.36 ± 0.02 L m^{-2} h^{-1}). The reported values are consistent with literature data for TFC membranes fabricated with low-to-moderate salt permeabilities, where average *B* ranges from 0.11 ± 0.04 to 0.76 ± 0.14 L m^{-2} h^{-1}.[64] On the other hand, the TFC-LBL membrane had a significantly higher salt permeability coefficient at 2.14 ± 0.36 L m^{-2} h^{-1}, nearly 6 times the control (Fig. 6B), suggesting that the *in situ* AgNP formation may have damaged the membrane polyamide layer due to exposure to the strong reducing agent $NaBH_4$.

FTIR-ATR analysis was conducted on the pristine and modified membranes to investigate the chemical bonds present on the membrane surface (Fig. S5†). The FTIR spectra for the unmodified TFC membrane and all modified membranes were found to be quite similar. However, there were slight differences in the intensity of the absorption band at 3420 cm^{-1}, which corresponds to the hydroxyl functional group (Fig. S5†). Instead, the greatest contribution to the absorption bands observed in the FTIR spectra is simply the polyamide selective layer itself. For these reasons, the modification of the TFC membrane surface with CNC and/or AgNP using the PDA self-polymerization reaction may not be readily distinguishable based on the FTIR spectra alone.

On the other hand, XPS analysis provided more detailed information on the chemical bonds present on the surface of the pristine TFC and modified membranes (Fig. S6 and S7, Table S1†). The XPS full survey spectra (Fig. S6†) show peaks for carbon, nitrogen, and oxygen for all the membranes. The presence of these elements results from the elemental composition of the polyamide selective layer on the TFC membranes. Carbon, nitrogen, and oxygen are all components of the amide bonds that are recurrent throughout the polymer structure of the polyamide selective layer. Notably, the TFC-OP and TFC-LBL membranes exhibited two peaks at a binding energy of ~375 eV, which is attributable to the presence of silver. In the higher resolution Ag 3d spectrum, the silver-attributable peaks can be observed as a doublet separated by 6.0 eV. This is observed for both the TFC-OP membrane (Fig. S7E†) and the TFC-LBL membrane (Fig. S7G†). The peak at a binding energy of 368.9 eV is attributed to Ag $3d_{5/2}$ while the peak at a binding energy of 374.9 eV is attributed to Ag $3d_{3/2}$. The 6.0 eV binding energy separating these two peaks is indicative of the presence of zero-valent silver.[61,62] The Ag 3d high-resolution spectrum for the TFC-OP and TFC-LBL membranes confirms the presence of metallic AgNP on the membrane surface, which results from the membrane modification processes. Additionally, oxygen-to-nitrogen (O/N) ratios calculated from the relative intensity of the peaks attributed to O 1s and N 1s (Fig. S6†) suggest a reduction in the crosslinking degree of the membranes as follows: pristine TFC (O/N = 1.08) > TFC-PDA (O/N = 1.09) > TFC-CNC (O/N = 1.16) > TFC-OP (O/N = 1.70) > TFC-LBL (O/N = 2.02). A theoretical O/N ratio of 1.0 implies a fully crosslinked polyamide layer, while a value of 2.0 indicates a fully linear layer.[65] Therefore, as observed before for membranes functionalized with metal–organic framework nanocrystals[66] or CNC,[67] the increase in the O/N ratio can be assigned to the formation of a less crosslinked structure in the polyamide network due to the immobilization of CNC and AgNP, or the presence of additional oxygen sources from the nanomaterials.

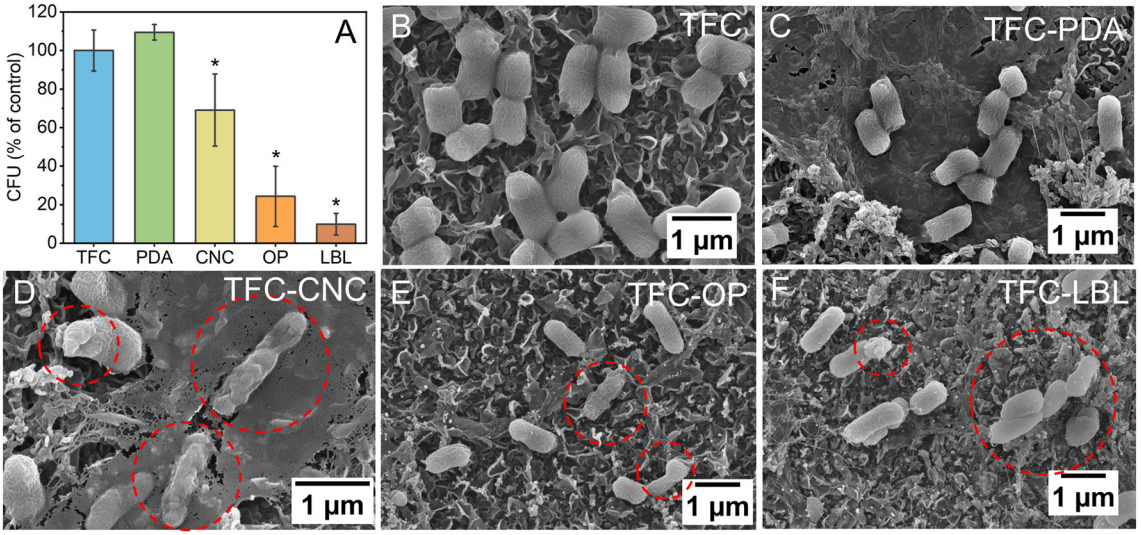

Fig. 7 (A) Antimicrobial properties of the pristine and modified membranes after exposure to *E. coli* cells for 3 h. An asterisk is used to denote samples that were statistically significantly different than the control at a confidence level of 95% (α = 0.05). SEM micrographs showing the cellular integrity of *E. coli* cells after exposure to the (B) pristine TFC membrane, (C) membrane modified with only PDA (TFC-PDA), (D) membrane modified with CNC using PDA (TFC-CNC), (E) membrane functionalized using "one-pot" method to attach CNC/Ag to the membrane surface with PDA (TFC-OP), and (F) membrane modified using the "layer-by-layer" method to attach CNC to the membrane *via* PDA followed by *in situ* AgNP formation (TFC-LBL). Morphological damage to the *E. coli* cells is indicated with a red circle.

Antimicrobial activity of functionalized membranes in static conditions

All functionalized membranes except for the membrane modified with only the thin layer of PDA demonstrated toxicity to *E. coli* after 3 hours of exposure to the membrane surface at room temperature (Fig. 7A). A reduction in viable cells of 30.9 ± 18.7% after 3 h of exposure was observed for the membranes modified with CNC. This was further improved by using the CNC in conjunction with AgNP. The TFC-OP and TFC-LBL membranes decreased the number of viable cells by 75.7 ± 15.6% and 90.1 ± 5.6%, respectively, after 3 h of exposure to the membrane surface. SEM micrographs provided further evidence of the damage caused to the bacteria by CNC and AgNP deposited on the membrane surface, as shown in Fig. 7. While the TFC-LBL was the best-performing membrane in terms of antimicrobial activity, the functionalization method employed for this membrane had an adverse effect on its salt rejection capability. Specifically, the TFC-LBL membrane demonstrated a salt permeability coefficient, B, that was 6 times higher than that of the control TFC membrane. The *in situ* application of AgNP to the membrane involved the use of $NaBH_4$ to convert silver ions, adsorbed onto the membrane surface, into Ag^0. However, this reaction may be overly aggressive and cause harm to the TFC membrane surface, ultimately leading to a reduction in the membrane performance. In contrast, the TFC-OP method does not require direct contact with $NaBH_4$, mitigating any potential risk to membrane transport properties. An overview of the key membrane parameters affected by the "one-pot" and "layer-by-layer" methods, in comparison to other approaches to obtain AgNP-functionalized membranes, is presented in Table S2.†

Static biofouling assays were also conducted using LB to encourage the growth of the *E. coli* cells attached to the membrane surface after a preliminary contact period of 3 h contact with the membrane surface, providing a condition that would offer extra challenge to the modified membranes. These membranes were stained with SYTO 9 to label live cells and PI to label dead cells. Confocal microscopy was employed to observe the labeled membranes. Confocal images depicted in Fig. S8† portray the distribution of live and dead *E. coli* cells on each membrane surface. The membranes containing silver displayed the highest proportion of dead cells, 71.4% and 73.5% of the total *E. coli* cells observed were dead on the TFC-OP and TFC-LBL, respectively (Table S3†). This result can be attributed to the broad-spectrum toxicity of AgNP and

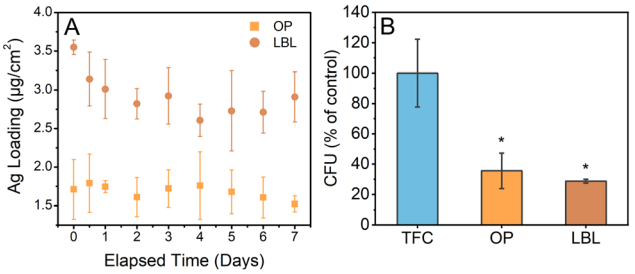

Fig. 8 (A) Concentration of silver ions leached from TFC-OP and TFC-LBL membranes into 5 mM $NaHCO_3$ over the course of 7 days. Silver concentrations were determined using ICP-MS. (B) Antimicrobial properties of the TFC-OP and TFC-LBL membranes following 14 days of leaching in 5 mM $NaHCO_3$ and exposure to *E. coli* cells for 3 h.

corroborates the toxicity observed on the membrane surface shown in Fig. 7A.

Antimicrobial properties of the functionalized membranes containing silver were also measured after silver leaching was performed in 5 mM $NaHCO_3$ solution (Fig. 8A and B). The results of the antimicrobial assays following silver leaching are shown in Fig. 8B. After 14 days of leaching, the TFC-OP and TFC-LBL membranes showed a reduction in the number of viable cells by 64.4 ± 11.7% and 71.3 ± 1.3%, respectively. This finding suggests that the membranes remained toxic to bacteria even after washing cycles, with TFC-LBL showing a slightly better antimicrobial activity compared with TFC-OP. Upon analyzing the membrane samples using ICP-MS, it was observed that the TFC-LBL membrane exhibited a higher initial deposit of silver compared to the TFC-OP membrane (Fig. 8A). The available silver leached more swiftly from the TFC-LBL than the TFC-OP membrane. The reason for this observation could be attributed to the nucleation of AgNP on CNC, which improves the stability of AgNP, thereby reducing the pace at which the metallic AgNP oxidizes and dissolves into the neighboring solution. The average Ag^+ leaching rate of TFC-OP, estimated as 0.027 μg cm^{-2} per day, is lower than that of deposited AgNP[68] and similar to the release rate observed in membranes modified with a hybrid nanomaterial consisting of tannic acid-functionalized carbon nanotubes embedded with *in situ* nucleated AgNP[69] (Table S3†).

Conclusions

Through biomimetic polydopamine chemistry, CNC and AgNP were attached to the TFC membrane surface using two different methods in aqueous media. In the "one-pot" method, a CNC/Ag hybrid nanomaterial was immobilized on the membrane surface in a single step, following an initial PDA layer. In the "layer-by-layer" method, CNC was applied to the membrane surface after an initial PDA layer, followed by the *in situ* anchoring of AgNP *via* the reduction of Ag^+ with $NaBH_4$. Both methods of functionalization did not significantly increase the membrane roughness or hydrophobicity but were effective in providing antimicrobial properties to the membrane surface. The TFC-LBL membrane exhibited the highest antimicrobial activity, deactivating up to 90% of attached *E. coli* cells in 3 hours, with a higher loading of available silver and a steeper leaching rate of Ag^+ over 7 days. However, the "layer-by-layer" approach affected the transport properties of the modified membrane, increasing the solute permeability coefficient *B* by 6 times compared to the pristine TFC membrane. This reduction in salt rejection is likely due to damage sustained by the selective active layer during the *in situ* deposition of AgNP. This highlights the need to optimize the LBL deposition method in future work to ensure minimal membrane damage and sufficient AgNP formation, thus enhancing the competitiveness of this method. Conversely, the "one-pot" method of applying CNC/Ag hybrid nanomaterial to the membrane surface was a more straightforward strategy, conferring antimicrobial activity without compromising the membrane transport properties, which is essential in large-scale application of water filtration and desalination. More specifically, the TFC-OP membrane deactivated up to 76% of attached *E. coli* cells in 3 hours without compromising the water or solute permeabilities (parameters *A* and *B*, respectively). The TFC-OP membrane presented a lower loading of Ag, a more sustained leaching rate of silver ions, and a statistically equivalent antimicrobial property to TFC-LBL after 14 days of leaching. Therefore, the "one-pot" method was shown to be more effective for producing TFC membranes with good antimicrobial properties concomitantly with sustainable efficiency for water treatment processes.

Author contributions

The manuscript was written through the contributions of all authors. All authors have approved the final version of the manuscript.

Conflicts of interest

The authors agree that there are no conflicts of interest to declare.

Acknowledgements

We would like to acknowledge UF ICBR Electron Microscopy, RRID:SCR_019146. Specifically, we would like to thank Nicole J. Machi and Karen Kelley for their assistance with this project by collecting TEM images. We would also like to acknowledge that the Nikon A1RMPsi used to collect confocal images was purchased as a part of NIH Grant #1S10OD020026. We would like to acknowledge and extend our gratitude to Doug Smith for his assistance collecting the confocal images. This study was financed in part by the São Paulo Research Foundation (FAPESP, grant number 2021/12071-6) and the National Council for Scientific and Technological Development (CNPq, grant number 151281/2022-0).

References

1 I. Delpla, A.-V. Jung, E. Baures, M. Clement and O. Thomas, Impacts of Climate Change on Surface Water Quality in Relation to Drinking Water Production, *Environ. Int.*, 2009, **35**(8), 1225–1233, DOI: **10.1016/J.ENVINT.2009.07.001**.
2 J. Beth Zimmerman, J. R. Mihelcic and J. Smith, Global Stressors on Water Quality and Quantity, *Environ. Sci. Technol.*, 2008, **42**(12), 4247–4254.
3 M. Elimelech, The Global Challenge for Adequate and Safe Water, *J. Water Supply: Res. Technol.–AQUA*, 2006, **55**(1), 3–10, DOI: **10.2166/aqua.2005.064**.

4 B. Sivakumar, Global Climate Change and Its Impacts on Water Resources Planning and Management: Assessment and Challenges, *Stochastic Environ. Res. Risk Assess.*, 2011, **25**(4), 583–600, DOI: **10.1007/S00477-010-0423-Y/FIGURES/3**.

5 C. J. Vörösmarty, P. Green, J. Salisbury and R. B. Lammers, Global Water Resources: Vulnerability from Climate Change and Population Growth, *Science*, 2000, **289**(5477), 284–288, DOI: **10.1126/science.289.5477.284**.

6 G. Liu, Y. Zhang, W. J. Knibbe, C. Feng, W. Liu, G. Medema and W. van der Meer, Potential Impacts of Changing Supply-Water Quality on Drinking Water Distribution: A Review, *Water Res.*, 2017, 135–148, DOI: **10.1016/j.watres.2017.03.031**.

7 T. A. Larsen, S. Hoffmann, C. Lüthi, B. Truffer and M. Maurer, Emerging Solutions to the Water Challenges of an Urbanizing World, *Science*, 2016, **352**(6288), 928–933, DOI: **10.1126/SCIENCE.AAD8641/ASSET/A9922F96-BEE1-463A-87D3-ACA9AE961B79/ASSETS/GRAPHIC/352_928_T2D.JPEG**.

8 S. Kerwin and B. T. Adey, Optimal Intervention Planning: A Bottom-Up Approach to Renewing Aging Water Infrastructure, *J. Water Resour. Plan. Manag.*, 2020, **146**(7), 04020044, DOI: **10.1061/(ASCE)WR.1943-5452.0001217/ASSET/2A2AFFF9-738E-4B9E-AE0F-C0AA47BEB366/ASSETS/IMAGES/LARGE/FIGURE11.JPG**.

9 L. M. Mosley, Drought Impacts on the Water Quality of Freshwater Systems; Review and Integration, *Earth-Sci. Rev.*, 2015, **140**, 203–214, DOI: **10.1016/J.EARSCIREV.2014.11.010**.

10 M. A. Shannon, P. W. Bohn, M. Elimelech, J. G. Georgiadis, B. J. Mariñas and A. M. Mayes, Science and Technology for Water Purification in the Coming Decades, in *Nanoscience and Technology*, Co-Published with Macmillan Publishers Ltd, UK, 2009, pp. 337–346, DOI: **10.1142/9789814287005_0035**.

11 Z. Zhang, Y. Su, J. Zhu, J. Shi, H. Huang and B. Xie, Distribution and Removal Characteristics of Microplastics in Different Processes of the Leachate Treatment System, *Waste Manage.*, 2021, **120**, 240–247, DOI: **10.1016/J.WASMAN.2020.11.025**.

12 K. S. Goh, Y. Chen, J. Y. Chong, T. H. Bae and R. Wang, Thin Film Composite Hollow Fibre Membrane for Pharmaceutical Concentration and Solvent Recovery, *J. Membr. Sci.*, 2021, **621**, 119008, DOI: **10.1016/J.MEMSCI.2020.119008**.

13 S. Basu and M. Balakrishnan, Polyamide Thin Film Composite Membranes Containing ZIF-8 for the Separation of Pharmaceutical Compounds from Aqueous Streams, *Sep. Purif. Technol.*, 2017, **179**, 118–125, DOI: **10.1016/J.SEPPUR.2017.01.061**.

14 S. Das and A. Ronen, A Review on Removal and Destruction of Per-and Polyfluoroalkyl Substances (PFAS) by Novel Membranes, *Membranes*, 2022, **12**(7), 662, DOI: **10.3390/MEMBRANES12070662/S1**.

15 M. N. Nadagouda and T. Lee, Cross-Flow Treatment of PFAS in Water: Materials Challenges and Potential Solutions, *Acc. Mater. Res.*, 2021, **2**(3), 129–133, DOI: **10.1021/accountsmr.0c00106**.

16 W. Chen, M. Liu, M. Ding, L. Zhang and S. Dai, Advanced Thin-Film Composite Polyamide Membrane for Precise Trace Short-Chain PFAS Sieving: Solution, Environment and Fouling Effects, *Process Saf. Environ. Prot.*, 2023, **169**, 493–503, DOI: **10.1016/J.PSEP.2022.11.036**.

17 S. F. E. Boerlage, M. Kennedy, M. P. Aniye and J. C. Schippers, Applications of the MFI-UF to Measure and Predict Particulate Fouling in RO Systems, *J. Membr. Sci.*, 2003, **220**(1–2), 97–116, DOI: **10.1016/S0376-7388(03)00222-9**.

18 S. G. Yiantsios, D. Sioutopoulos and A. J. Karabelas, Colloidal Fouling of RO Membranes: An Overview of Key Issues and Efforts to Develop Improved Prediction Techniques, *Desalination*, 2005, **183**(1–3), 257–272, DOI: **10.1016/J.DESAL.2005.02.052**.

19 T. Tong, A. F. Wallace, S. Zhao and Z. Wang, Mineral Scaling in Membrane Desalination: Mechanisms, Mitigation Strategies, and Feasibility of Scaling-Resistant Membranes, *J. Membr. Sci.*, 2019, **579**, 52–69, DOI: **10.1016/J.MEMSCI.2019.02.049**.

20 C. S. Ong, P. S. Goh, W. J. Lau, N. Misdan and A. F. Ismail, Nanomaterials for Biofouling and Scaling Mitigation of Thin Film Composite Membrane: A Review, *Desalination*, 2016, **393**, 2–15, DOI: **10.1016/j.desal.2016.01.007**.

21 Q. Li and M. Elimelech, Organic Fouling and Chemical Cleaning of Nanofiltration Membranes: Measurements and Mechanisms, *Environ. Sci. Technol.*, 2004, **38**(17), 4683–4693, DOI: **10.1021/es0354162**.

22 M. Xie, J. Lee, L. D. Nghiem and M. Elimelech, Role of Pressure in Organic Fouling in Forward Osmosis and Reverse Osmosis, *J. Membr. Sci.*, 2015, **493**, 748–754, DOI: **10.1016/J.MEMSCI.2015.07.033**.

23 H.-C. Flemming, G. Schaule, T. Griebe, J. Schmitt and A. Tamachkiarowa, Biofouling—the Achilles Heel of Membrane Processes, *Desalination*, 1997, **113**(2–3), 215–225, DOI: **10.1016/S0011-9164(97)00132-X**.

24 H. Maddah and A. Chogle, Biofouling in Reverse Osmosis: Phenomena, Monitoring, Controlling and Remediation, *Appl. Water Sci.*, 2016, **7**(6), 2637–2651, DOI: **10.1007/S13201-016-0493-1**.

25 C. Dreszer, J. S. Vrouwenvelder, A. H. Paulitsch-Fuchs, A. Zwijnenburg, J. C. Kruithof and H.-C. Flemming, Hydraulic Resistance of Biofilms, *J. Membr. Sci.*, 2013, **429**, 436–447, DOI: **10.1016/J.MEMSCI.2012.11.030**.

26 D. Davies, Understanding Biofilm Resistance to Antibacterial Agents, *Nat. Rev. Drug Discovery*, 2003, **2**(2), 114–122, DOI: **10.1038/nrd1008**.

27 G. Ye, J. Lee, F. Perreault and M. Elimelech, Controlled Architecture of Dual-Functional Block Copolymer Brushes on Thin-Film Composite Membranes for Integrated "Defending" and "Attacking" Strategies against Biofouling, *ACS Appl. Mater. Interfaces*, 2015, **7**(41), 23069–23079, DOI: **10.1021/acsami.5b06647**.

28 A. Rahimi and H. Mahdavi, Zwitterionic-Functionalized GO/PVDF Nanocomposite Membranes with Improved Anti-Fouling Properties, *J. Water Process Eng.*, 2019, **32**, 100960, DOI: **10.1016/j.jwpe.2019.100960**.

29 P. Bengani-Lutz, E. Converse, P. Cebe and A. Asatekin, Self-Assembling Zwitterionic Copolymers as Membrane Selective Layers with Excellent Fouling Resistance: Effect of Zwitterion Chemistry, *ACS Appl. Mater. Interfaces*, 2017, **9**(24), 20859–20872, DOI: **10.1021/acsami.7b04884**.

30 M. B. Gohain, R. R. Pawar, S. Karki, A. Hazarika, S. Hazarika and P. G. Ingole, Development of Thin Film Nanocomposite Membrane Incorporated with Mesoporous Synthetic Hectorite and MSH@UiO-66-NH2 Nanoparticles for Efficient Targeted Feeds Separation, and Antibacterial Performance, *J. Membr. Sci.*, 2020, **609**, 118212, DOI: **10.1016/j.memsci.2020.118212**.

31 S. Karki, M. B. Gohain, D. Yadav, N. R. Thakare, R. R. Pawar, S. Hazarika and P. G. Ingole, Building Rapid Water Transport Channels within Thin-Film Nanocomposite Membranes Based on 2D Mesoporous Nanosheets, *Desalination*, 2023, **547**, 116222, DOI: **10.1016/j.desal.2022.116222**.

32 S. Kang, M. Herzberg, D. F. Rodrigues and M. Elimelech, Antibacterial Effects of Carbon Nanotubes: Size Does Matter!, *Langmuir*, 2008, **24**(13), 6409–6413, DOI: **10.1021/la800951v**.

33 C. Yang, J. Mamouni, Y. Tang and L. Yang, Antimicrobial Activity of Single-Walled Carbon Nanotubes: Length Effect, *Langmuir*, 2010, **26**(20), 16013–16019, DOI: **10.1021/la103110g**.

34 A. F. Faria, F. Perreault and M. Elimelech, Elucidating the Role of Oxidative Debris in the Antimicrobial Properties of Graphene Oxide, *ACS Appl. Nano Mater.*, 2018, **1**(3), 1164–1174, DOI: **10.1021/acsanm.7b00332**.

35 F. Perreault, A. Fonseca de Faria and M. Elimelech, Environmental Applications of Graphene-Based Nanomaterials, *Chem. Soc. Rev.*, 2015, **44**(16), 5861–5896, DOI: **10.1039/C5CS00021A**.

36 A. F. De Faria, F. O. Perreault, E. Shaulsky, L. H. Arias Chavez and M. Elimelech, Antimicrobial Electrospun Biopolymer Nanofiber Mats Functionalized with Graphene Oxide–Silver Nanocomposites, *ACS Appl. Mater. Interfaces*, 2015, **7**(23), 12751–12759, DOI: **10.1021/acsami.5b01639**.

37 A. Tiraferri, C. D. Vecitis and M. Elimelech, Covalent Binding of Single-Walled Carbon Nanotubes to Polyamide Membranes for Antimicrobial Surface Properties, *ACS Appl. Mater. Interfaces*, 2011, **3**(8), 2869–2877, DOI: **10.1021/am200536p**.

38 V. T. Noronha, C. H. M. Camargos, J. C. Jackson, A. G. Souza Filho, A. J. Paula, C. A. Rezende and A. F. Faria, Physical Membrane-Stress-Mediated Antimicrobial Properties of Cellulose Nanocrystals, *ACS Sustainable Chem. Eng.*, 2021, **9**(8), 3203–3212, DOI: **10.1021/acssuschemeng.0c08317**.

39 J. C. Jackson, C. H. M. Camargos, V. T. Noronha, A. J. Paula, C. A. Rezende and A. F. Faria, Sustainable Cellulose Nanocrystals for Improved Antimicrobial Properties of Thin Film Composite Membranes, *ACS Sustainable Chem. Eng.*, 2021, **9**(19), 6534–6540, DOI: **10.1021/acssuschemeng.1c02389**.

40 V. T. Noronha, J. C. Jackson, C. H. M. Camargos, A. J. Paula, C. A. Rezende and A. F. Faria, "Attacking–Attacking" Anti-Biofouling Strategy Enabled by Cellulose Nanocrystals–Silver Materials, *ACS Appl. Bio Mater.*, 2022, **5**(3), 1025–1037, DOI: **10.1021/acsabm.1c00929**.

41 H. H. Tuson and D. B. Weibel, Bacteria–Surface Interactions, *Soft Matter*, 2013, **9**(17), 4368–4380, DOI: **10.1039/C3SM27705D**.

42 L. Fan, H. Zhang, M. Gao, M. Zhang, P. Liu and X. Liu, Cellulose Nanocrystals/Silver Nanoparticles: In-Situ Preparation and Application in PVA Films, *Holzforschung*, 2020, **74**(5), 523–528, DOI: **10.1515/hf-2018-0251**.

43 N. Drogat, R. Granet, V. Sol, A. Memmi, N. Saad, C. Klein Koerkamp, P. Bressollier and P. Krausz, Antimicrobial Silver Nanoparticles Generated on Cellulose Nanocrystals, *J. Nanopart. Res.*, 2011, **13**(4), 1557–1562, DOI: **10.1007/s11051-010-9995-1**.

44 B. Le Ouay and F. Stellacci, Antibacterial Activity of Silver Nanoparticles: A Surface Science Insight, *Nano Today*, 2015, **10**(3), 339–354, DOI: **10.1016/j.nantod.2015.04.002**.

45 S. Prabhu and E. K. Poulose, Silver Nanoparticles: Mechanism of Antimicrobial Action, Synthesis, Medical Applications, and Toxicity Effects, *Int. Nano Lett.*, 2012, **2**(1), 1–10, DOI: **10.1186/2228-5326-2-32**.

46 J. R. Morones, J. L. Elechiguerra, A. Camacho, K. Holt, J. B. Kouri, J. T. Ramírez and M. J. Yacaman, The Bactericidal Effect of Silver Nanoparticles, *Nanotechnology*, 2005, **16**(10), 2346, DOI: **10.1088/0957-4484/16/10/059**.

47 K. M. M. Abou El-Nour, A. Eftaiha, A. Al-Warthan and R. A. A. Ammar, Synthesis and Applications of Silver Nanoparticles, *Arabian J. Chem.*, 2010, **3**(3), 135–140, DOI: **10.1016/j.arabjc.2010.04.008**.

48 T. C. Dakal, A. Kumar, R. S. Majumdar and V. Yadav, Mechanistic Basis of Antimicrobial Actions of Silver Nanoparticles, *Front. Microbiol.*, 2016, **7**(Nov), 1831, DOI: **10.3389/FMICB.2016.01831/BIBTEX**.

49 J. Lv, X. Zhang, N. Yu, S. Su, J. Zhu, L. Deng and Z. Liu, One-Pot Synthesis of CNC-Ag@AgCl with Antifouling and Antibacterial Properties, *Cellulose*, 2019, **26**(13–14), 7837–7846, DOI: **10.1007/S10570-019-02658-9/FIGURES/5**.

50 K. Liu, H. Liang, J. Nasrallah, L. Chen, L. Huang and Y. Ni, Preparation of the CNC/Ag/Beeswax Composites for Enhancing Antibacterial and Water Resistance Properties of Paper, *Carbohydr. Polym.*, 2016, **142**, 183–188, DOI: **10.1016/J.CARBPOL.2016.01.044**.

51 L. Du, K. Arnholt, S. Ripp, G. Sayler, S. Wang, C. Liang, J. Wang and J. Zhuang, Biological Toxicity of Cellulose Nanocrystals (CNCs) against the LuxCDABE-Based Bioluminescent Bioreporter Escherichia Coli 652T7, *Ecotoxicology*, 2015, **24**(10), 2049–2053, DOI: **10.1007/s10646-015-1555-0**.

52 J. He, T. Kunitake and A. Nakao, Facile In Situ Synthesis of Noble Metal Nanoparticles in Porous Cellulose Fibers, *Chem. Mater.*, 2003, **15**(23), 4401–4406, DOI: **10.1021/cm034720r**.

53 D. Caschera, R. G. Toro, F. Federici, R. Montanari, T. de Caro, M. T. Al-Shemy and A. M. Adel, Green Approach for

the Fabrication of Silver-Oxidized Cellulose Nanocomposite with Antibacterial Properties, *Cellulose*, 2020, **27**(14), 8059–8073, DOI: **10.1007/s10570-020-03364-7**.

54 D. Musino, C. Rivard, G. Landrot, B. Novales, T. Rabilloud and I. Capron, Hydroxyl Groups on Cellulose Nanocrystal Surfaces Form Nucleation Points for Silver Nanoparticles of Varying Shapes and Sizes, *J. Colloid Interface Sci.*, 2021, **584**, 360–371, DOI: **10.1016/J.JCIS.2020.09.082**.

55 C. H. M. Camargos and C. A. Rezende, Structure–Property Relationships of Cellulose Nanocrystals and Nanofibrils: Implications for the Design and Performance of Nanocomposites and All-Nanocellulose Systems, *ACS Appl. Nano Mater.*, 2021, **4**(10), 10505–10518, DOI: **10.1021/acsanm.1c02008**.

56 H. Liu, D. Wang, Z. Song and S. Shang, Preparation of Silver Nanoparticles on Cellulose Nanocrystals and the Application in Electrochemical Detection of DNA Hybridization, *Cellulose*, 2011, **18**(1), 67–74, DOI: **10.1007/s10570-010-9464-0**.

57 X. Xu, Y. Q. Yang, Y. Y. Xing, J. F. Yang and S. F. Wang, Properties of Novel Polyvinyl Alcohol/Cellulose Nanocrystals/Silver Nanoparticles Blend Membranes, *Carbohydr. Polym.*, 2013, **98**(2), 1573–1577, DOI: **10.1016/j.carbpol.2013.07.065**.

58 H. Lee, S. M. Dellatore, W. M. Miller and P. B. Messersmith, Mussel-Inspired Surface Chemistry for Multifunctional Coatings, *Science*, 2007, **318**(5849), 426–430, DOI: **10.1126/science.1147241**.

59 W. Cheng, X. Lu, M. Kaneda, W. Zhang, R. Bernstein, J. Ma and M. Elimelech, Graphene Oxide-Functionalized Membranes: The Importance of Nanosheet Surface Exposure for Biofouling Resistance, *Environ. Sci. Technol.*, 2020, **54**(1), 517–526, DOI: **10.1021/acs.est.9b05335**.

60 C. Liu, A. F. Faria, J. Jackson, Q. He and J. Ma, Enhancing the Anti-Fouling and Fouling Removal Properties of Thin-Film Composite Membranes through an Intercalated Functionalization Method, *Environ. Sci. Water Res. Technol.*, 2021, **7**(7), 1336–1347, DOI: **10.1039/D1EW00188D**.

61 Z. Ma, J. Liu, G. Shen, X. Zheng, Y. Pei and K. Tang, In-Situ Synthesis and Immobilization of Silver Nanoparticles on Microfibrillated Cellulose for Long-Term Antibacterial Applications, *Cellulose*, 2021, **28**(10), 6287–6303, DOI: **10.1007/S10570-021-03941-4/FIGURES/10**.

62 J. Zhu, T. Tang, C. Y. Hu, W. C. Xiang, Z. Q. Chen, L. Luo, H. S. Yang and H. P. Liu, Cellulose Nanocrystal Assisted Trace Silver Nitrate to Synthesize Green Silver Nanocomposites with Antibacterial Activity, *RSC Adv.*, 2021, **11**(7), 3808–3815, DOI: **10.1039/D0RA07198F**.

63 M. Elimelech and W. A. Phillip, The Future of Seawater Desalination: Energy, Technology, and the Environment, *Science*, 2011, **333**(6043), 712–717.

64 N. Y. Yip, A. Tiraferri, W. A. Phillip, J. D. Schiffman, L. A. Hoover, Y. C. Kim and M. Elimelech, Thin-Film Composite Pressure Retarded Osmosis Membranes for Sustainable Power Generation from Salinity Gradients, *Environ. Sci. Technol.*, 2011, **45**(10), 4360–4369, DOI: **10.1021/es104325z**.

65 Z. C. Ng, W. J. Lau, T. Matsuura and A. F. Ismail, Thin Film Nanocomposite RO Membranes: Review on Fabrication Techniques and Impacts of Nanofiller Characteristics on Membrane Properties, *Chem. Eng. Res. Des.*, 2021, **165**, 81–105, DOI: **10.1016/j.cherd.2020.10.003**.

66 A. Zirehpour, A. Rahimpour, A. Arabi Shamsabadi, M. G. Sharifian and M. Soroush, Mitigation of Thin-Film Composite Membrane Biofouling via Immobilizing Nano-Sized Biocidal Reservoirs in the Membrane Active Layer, *Environ. Sci. Technol.*, 2017, **51**(10), 5511–5522, DOI: **10.1021/acs.est.7b00782**.

67 J. J. Wang, H. C. Yang, M. B. Wu, X. Zhang and Z. K. Xu, Nanofiltration Membranes with Cellulose Nanocrystals as an Interlayer for Unprecedented Performance, *J. Mater. Chem. A*, 2017, **5**(31), 16289–16295, DOI: **10.1039/c7ta00501f**.

68 J. Yin, Y. Yang, Z. Hu and B. Deng, Attachment of Silver Nanoparticles (AgNPs) onto Thin-Film Composite (TFC) Membranes through Covalent Bonding to Reduce Membrane Biofouling, *J. Membr. Sci.*, 2013, **441**, 73–82, DOI: **10.1016/J.MEMSCI.2013.03.060**.

69 A. Zhao, N. Zhang, Q. Li, L. Zhou, H. Deng, Z. Li, Y. Wang, E. Lv, Z. Li, M. Qiao and J. Wang, Incorporation of Silver-Embedded Carbon Nanotubes Coated with Tannic Acid into Polyamide Reverse Osmosis Membranes toward High Permeability, Antifouling, and Antibacterial Properties, *ACS Sustainable Chem. Eng.*, 2021, **9**(34), 11388–11402, DOI: **10.1021/ACSSUSCHEMENG.1C03313/ASSET/IMAGES/LARGE/SC1C03313_0013.JPEG**.